Semiconductor Physics, Quantum Electronics & Optoelectronics, 2014. V. 17, N 3. P. 275-283.

PACS 61.05.cp, 64.75.St, 78.30.Fs, 79.60.-i

Optical and structural studies of phase transformations and composition fluctuations at annealing of $Zn_{1-x}Cd_xO$ films grown by dc magnetron sputtering

O. Kolomys[1,*], A. Romanyuk[1], V. Strelchuk[1], G. Lashkarev[2], O. Khyzhun[2], I. Timofeeva[2], V. Lazorenko[2], V. Khomyak[3]

[1] *V. Lashkaryov Institute of Semiconductor Physics, NAS of Ukraine, 41, prospect Nauky, 03028 Kyiv, Ukraine*

[*] *Corresponding author phone/fax: +38 (044)-525-6473; e-mail: olkolomys@gmail.com*

[2] *I. Frantsevich Institute for Problems of Materials Science, NAS of Ukraine, 3, Krzhizhanovsky str., 03680 Kyiv, Ukraine*

[3] *Chernivtsi National University, 2, Kotsiubinsky str., 58012 Chernivtsi, Ukraine*

Abstract. Ternary $Zn_{1-x}Cd_xO$ ($x \le 0.12$) alloy crystalline films with highly preferred orientation (002) have been successfully deposited on sapphire c-Al_2O_3 substrates using the direct current (dc) reactive magnetron sputtering technique and annealed at temperature 600 °C in air. The structural and optical properties of $Zn_{1-x}Cd_xO$ thin films were systematically studied using X-ray photoelectron spectroscopy (XPS), X-ray diffraction (XRD), micro-Raman and photoluminescent (PL) spectroscopy. XPS measurements clearly confirmed Cd incorporation into ZnO lattice. XRD data revealed that the growth of wurtzite $Zn_{1-x}Cd_xO$ films occurs preferentially in the (002) direction. Also, when the Cd content is increased, the XRD peaks shift towards smaller angles and the full width at half-maximum of the lines increases. When the Cd content increases, A_1^{LO} ($Zn_{1-x}Cd_xO$)-like Raman modes show composition dependent frequency decrease and asymmetrical broadening. The near band-edge PL emission at room temperature shifts gradually to lower energies as the Cd content increases and reaches 2.68 eV for the highest Cd content ($x = 0.12$). The analysis of NBE band emission and Raman A_1^{LO} ($Zn_{1-x}Cd_xO$) mode shows that at a higher Cd content the coexistence of $Zn_{1-x}Cd_xO$ areas with different concentrations of Cd inside the same film occurs. The presence of CdO in annealed $Zn_{1-x}Cd_xO$ films with the higher Cd content was confirmed by Raman spectra of cubic CdO nanoinclusions. The XRD data also revealed phase segregation of cubic CdO in annealed $Zn_{1-x}Cd_xO$ films (T_{ann} = 600 °C) for $x \ge 0.013$.

Keywords: $Zn_{1-x}Cd_xO$ films, XRD, XPS, Raman spectroscopy, photoluminescence, phase segregation.

Manuscript received 07.03.14; revised version received 27.06.14; accepted for publication 16.09.14; published online 30.09.14.

1. Introduction

Wurtzite ZnO semiconductor is perspective material for short-wave light emitting/detecting optoelectronic devices even at room temperature due to its wide direct band gap 3.34 eV, high exciton binding energy (~60 meV) and satisfactory electron mobility [1]. An important issue to design ZnO-based devices is the growth and characterization of high quality $Zn_{1-x}Cd_xO$ ternary alloys for band-gap engineering. The band gap of $Zn_{1-x}Cd_xO$ can be potentially tuned within the range from 3.4 eV ($x = 0$) down to 2.28 eV (CdO) [2]. Up to date, the properties of $Zn_{1-x}Cd_xO$ alloys have not yet been studied completely. Furthermore, because of the different crystallographic structures of the outermost

binary compounds ZnO and CdO – wurtzite (wz) and rocksalt (rs), respectively, the growth of single-phase $Zn_{1-x}Cd_xO$ alloys over the full compositional range is impossible. Solubility of Cd in ZnO is limited up to $x = 0.04$ in equilibrium growth conditions [3]. But higher Cd concentrations can be obtained growing $Zn_{1-x}Cd_xO$ in conditions far from the equilibrium ones, and thus compositions up to $x = 0.70$ have been achieved [4]. It was shown that ternary $Zn_{1-x}Cd_xO$ alloy have a stable single-phase wz structure at $x < 0.02$, while at the higher Cd content ($0.07 < x < 0.17$), phase separation by wz, zb and rs structural phases occurs [5]. The Cd-rich and Cd-poor nanodomains were observed in microscopic cathodoluminescence spectra of $Zn_{1-x}Cd_xO$ epilayers with the higher Cd content [6]. It is very important to optimize amount of Cd, which could be dissolved in ZnO thin films without phase segregation, with minimum in the amount of defects and good crystal quality. It was demonstrated that post-growth rapid thermal annealing (RTA) allows to obtain single-phase $Zn_{1-x}Cd_xO$ alloys, improve their crystal quality [7, 8], and reduce a density of native point defects [9, 10].

Raman spectroscopy is a fast, contactless and nondestructive technique for studying microstructural disorder, phase composition and degree of inhomogeneity in particular for ternary A^2B^6-based alloys. However, vibrational properties of $Zn_{1-x}Cd_xO$ have not been extensively investigated. To the best of our knowledge, there is no Raman study of the $Zn_{1-x}Cd_xO$ films containing different structural phases simultaneously.

In this work, the influence of Cd doping on structure, phase, composition and optical properties of $Zn_{1-x}Cd_xO$ thin films deposited using the dc reactive magnetron sputtering technique was studied. The chemical state of Zn and O as well as composition of the surface of $Zn_{1-x}Cd_xO$ films were determined by studying the XPS data of as-grown films. XRD studies confirm that all the films exhibit the patterns that are typical for the wurtzite structure. The effects of varying the Cd content and temperature annealing on the optical properties of the films have been investigated using XRD, micro-Raman scattering and photoluminescence (PL). An increase in the Cd content leads to the coexistence of areas with different composition within the same $Zn_{1-x}Cd_xO$ film. The near band-edge (NBE) PL peak showed red shift and broadening with the Cd content increase, giving a strong evidence of band-gap shrinkage and deterioration of crystallinity due to Cd incorporation. After annealing, two separated NBE PL peaks and two Raman A_1^{LO} modes are observed, which correspond to different possible structural phases of $Zn_{1-x}Cd_xO$. The presence of high-frequency E_2^{high} mode and longitudinal optical A_1^{LO} modes in the Raman spectra confirms the hexagonal wurtzite structure of the films. For annealed $Zn_{1-x}Cd_xO$ films with the higher Cd-content, the presence of metastable cubic CdO nanophase in $Zn_{1-x}Cd_xO$ layer is confirmed by the XRD data and Raman spectra [11].

2. Experimental

The 1.6-μm thick $Zn_{1-x}Cd_xO$ films ($x \le 0.12$) were grown on sapphire substrates at 400 °C by using the direct current (dc) magnetron sputtering technique for reactive deposition. The dc sputtering system operates using Zn-Cd metal alloy of 99.99% purity as a sputtering target. The target diameter was 10 cm. The cadmium content in these films was controlled changing the deposition conditions (ratio of partial pressures of argon and oxygen; dc power). We used DRON-4 diffractometer (operating at 40 kV and 30 mA) with a Cu Kα radiation source ($\lambda = 0.154056$ nm) to investigate crystal quality and crystal structure of as-grown and annealed films for identification the chemical state of Zn, O and their ratio. The scan rate 1°/min and step size 0.01° were used. The XPS measurements were performed using the UHV-Analysis-System assembled by the SPECS (Germany) equipped with a PHOIBOS 150 hemispherical analyzer and monochromatic Al$K\alpha$ (E = 1486.6 eV) radiation source. The XPS analysis chamber was evacuated to less than $9 \cdot 10^{-8}$ Pa. The XPS spectra were measured at the constant incident energy of 25 eV. The binding energy (BE) 84.00±0.05 eV of the XPS Au $4f_{7/2}$ core-level spectrum was used as a reference. When determining binding energies, the accuracy was ±0.05 eV. The micro-Raman spectra of $Zn_{1-x}Cd_xO$ films were recorded in backscattering geometry at room temperature (RT) by using the Horiba Jobin-Yvon T64000 spectrometer equipped with a CCD detector. The spectral resolution was about $0.15\,cm^{-1}$. The experiments were carried out with the 488.0-nm line of an Ar/Kr laser for non-resonant excitation conditions, and with the 325.0-nm line of an He-Cd laser for the resonant ones. The excitation wavelength chosen for PL excitation was 325 nm ($E_{exc} \approx 3.81$ eV). A 50× objective was used to focus the laser beam and collect backscattered light. The annealing treatment of samples was performed in a silica tube in air ambient at 600 °C for 1 hour.

3. Results and discussion

The XRD patterns of the as-grown and annealed $Zn_{1-x}Cd_xO$ films with the Cd content varying from $x = 0$ up to 0.12 are shown in Fig. 1. We could observe that XRD peaks of the as-grown ZnO film are at $2\theta = 35.0°$, 36.7° and 47.5°, which correspond to (002), (101) and (102) planes of typical wurtzite structure (JCPDS Card 36-1451). The shift of ZnO-related XRD peaks towards

higher angles with respect to those of bulk ZnO (see Table) indicates that the deposited films are under compressive strains. For $Zn_{1-x}Cd_xO$ films, the ω-2θ scan revealed that all the as-grown films had ZnO wurtzite structure, and signs of any secondary structural phase were not detected. We also noted in Fig. 1 that for as-grown samples (black lines) a weak shift of (002) peaks to small angles with increasing the Cd content was observed. It was found that the lattice parameter increased from 5.128 (x = 0) up to 5.273 Å (x = 0.117) due to replacement of Zn^{2+} (0.60 Å) by Cd^{2+} ions (0.75 Å) of comparatively larger size in the host ZnO crystal lattice [12]. The full width at half-maximum (FWHMs) for (002) XRD peak increases with Cd content enlargement (Table) indicating deterioration of the crystalline quality of the films due to increasing inhomogeneous microstrains (which can be obliged to fluctuations of Cd composition [13]) as well as to a decrease in the average dimensions inherent to coherently scattering areas (D) with an increase in the Cd content.

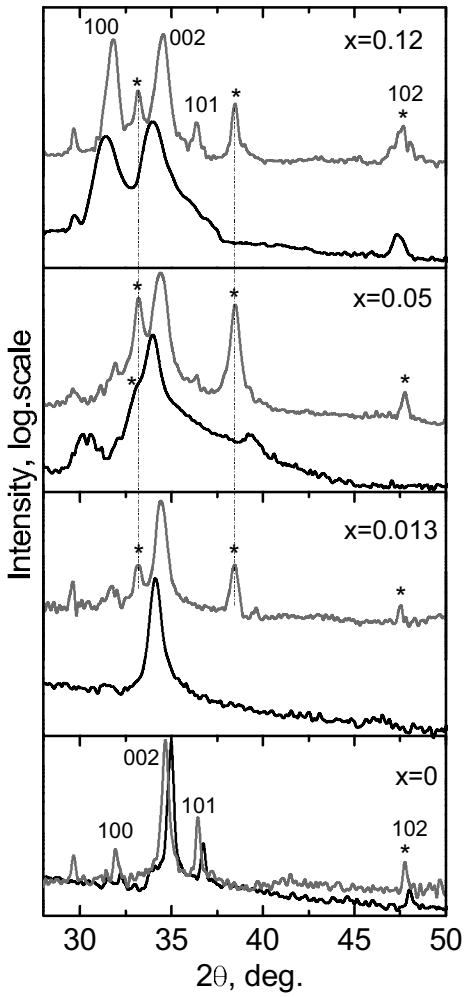

Fig. 1. XRD patterns for the as-grown (red (top) curves) and annealed (black (bottom) curves) $Zn_{1-x}Cd_xO$ films with the Cd content varying from x = 0.0 up to 0.12. The asterisks mark the cubic CdO-related peaks.

The XRD patterns of ZnO and $Zn_{1-x}Cd_xO$ as-grown and annealed films in the ambient air are shown in Fig. 1. It is important to note that thermal annealing of undoped ZnO film leads to the shift of the (002) peak to lower angles due to strain relaxation. Also, one can see the decrease in the FWHM value for ZnO and $Zn_{1-x}Cd_xO$ (002) diffraction peaks, which clearly means that the crystallite quality of ZnO and $Zn_{1-x}Cd_xO$ films is improved after annealing (see Table).

For annealed $Zn_{1-x}Cd_xO$ films, the ZnO-related XRD (002) peaks significantly shift towards higher angles and lattice parameter *c* decrease (Table). The latter can be consequently related to the diffusion of cadmium out of the film, as reported by Amanpal Singh et al. [14]. But as we can see from XRD patterns, the additional peaks from (111), (200) and (220) planes corresponding to cubic CdO (JCPDS no. 05-0640) appear after thermal annealing. It testifies to phase segregation with creation of cubic CdO. It is clearly observed that with increasing the Cd content up to x = 0.049, the intensity of the corresponding XRD peaks increased, which is indicative of the enlargement of CdO cubic phase content. In the case of the film with the Cd content of 11.9 at.%, the amount of separate CdO phase is slightly decreased as compared to that of the films with x = 0.013 and 0.049. It may be explained by disappearance of the preferred orientation at the high Cd content and enlargement of the amount of disordered (or amorphous) CdO phase.

To understand the nature of the phase composition inherent to the films, XPS spectra were measured for all the samples. Fig. 2 gives the wide-scan XPS spectra of $Zn_{1-x}Cd_xO$ samples with a different Cd content.

The atomic content of the Cd in $Zn_{1-x}Cd_xO$ films was determined using the integrated area under Cd $3d_{5/2}$, Zn $2p_{3/2}$ and O 1s principal peaks [15]. Fig. 3 shows the dependence of the integral area of the Cd $3d_{5/2}$ peak on the Cd content. It is worth noting that the Cd $3d_{5/2}$ peak exhibits a symmetrical shape indicating that the majority of Cd exists in the form of Cd^{2+} ions (Cd-O-Cd and Cd-O-Zn complexes).

The micro-Raman spectroscopy was applied to investigate structural properties, identify the composition variation and structural phase transformation in the $Zn_{1-x}Cd_xO$ films. Raman and PL micro-spectroscopy measurements were carried out from the same local area of the samples, which allowed obtaining simultaneous information about their crystalline and electron structure.

The wurtzite-type ZnO belongs to the space group C_{6v}^4 with two formula units in the primitive cell. The zone-center optical phonons can be classified according to the following irreducible representations: $\Gamma_{opt} = A_1 + E_1 + 2E_2 + 2B_1$ [16]. B_1 modes are the silent ones, A_1 and E_1 – polar modes that are both Raman and infrared active, whereas E_2 modes are non-polar and active only in Raman spectra. The symmetry-allowed Raman modes

Table. Structural parameters of $Cd_xZn_{1-x}O$ samples obtained from XRD data.

Cd content, x	$2\theta_{002}$, deg.		Lattice parameter *c*, nm		$FWHM_{002}$, deg.		Crystallite size *D*, nm	
	As-grown	Annealed	As-grown	Annealed	As-grown	Annealed	As-grown	Annealed
0	34.96	34.65	0.5128	0.5173	0.198	0.181	44	48
0.013	34.12	34.42	0.5250	0.5206	0.551	0.376	15	23
0.05	33.97	34.54	0.5273	0.5189	0.468	0.387	18	22
0.012	33.99	34.52	0.5270	0.5192	1.103	0.391	7	22

*Note. The experimental parameters presented in Table were compared to the XRD data for bulk ZnO ($2\theta_{002} = 34.42$, $c = 0.5207$) according to JCPDS Card 36-1451.

for the backscattering considered in this work are E_2^{high}, E_2^{low} and A_1^{LO} modes.

The near resonance of the incident or outgoing radiation with the electron states leads to the appearance of numerous replicas of the LO phonon modes, the number, intensity and FWHM of which are indicative of material quality and electron-phonon coupling [17]. Fig. 4 shows the multi-LO-phonon resonant Raman spectra (RRS) of as-grown ZnO and Cd-doped $Zn_{1-x}Cd_xO$ films excited with the 325-nm line of He-Cd laser (3.81 eV). This excitation energy is about 440 meV higher than the band gap of ZnO (3.34 eV) and matches the incoming resonance conditions with real interband electron transitions in these materials. In this case, the resonant enhancement of scattering of the multiple LO-phonon of A_1 symmetry (A_1^{LO}-band) in ZnO occurs even to the third order, which is caused by the strong intraband Fröhlich electron-phonon interaction [18]. In the resonant Raman spectra of the mentioned undoped ZnO sample, A_1^{LO}-bands at approximately 575.1 and 574.3 cm^{-1} were registered for as-grown and annealed ZnO films (Fig. 4a,b), respectively, and these bands are substantially broadened ($\Gamma \approx 30-31 cm^{-1}$), which is induced by inhomogeneous micro-strains as well as by fluctuations of the Cd content. The observed low-frequency shift of A_1^{LO}-band ($\Delta\omega \approx 0.8 cm^{-1}$) for the annealed ZnO film (as compared to the as-grown ZnO ones) is caused by relaxation of elastic compressive strains in the film during its thermal annealing. The presence of compressive strains in the as-grown ZnO film and their relaxation at annealing are in accordance with the XRD data.

When increasing the Cd content (to x = 0.12) in as-grown $Zn_{1-x}Cd_xO$ films, the small low-frequency shift of A_1^{LO}-band ($\Delta\omega(A_1^{LO}) \approx 1 cm^{-1}$) takes place. At the same time, after thermal annealing the value of low-frequency shift increases substantially ($\Delta\omega(A_1^{LO}) \approx 13 cm^{-1}$). In general, the low-frequency shift of $A_1(LO)$ phonon mode can be caused by an increase in the Cd concentration as well as by appearance of substantial elastic tensile strains. As it was mentioned above, the relaxation of elastic strains induces an insignificant A_1^{LO}-band frequency shift, thus we can conclude that in the annealed $Zn_{1-x}Cd_xO$ films the frequency change $\Delta\omega(A_1^{LO}) \approx 13 cm^{-1}$ can be mainly attributed to the Cd concentration increase in the film. Up to date, there are no literature data corresponding to compositional dependences of the phonon frequency for $Zn_{1-x}Cd_xO$ solid solution. If one suppose that for wurtzite $Zn_{1-x}Cd_xO$, the compositional dependence of the frequency has linear character, then the frequency of LO($Zn_{1-x}Cd_xO$) mode changes from ω_{LO}(wz-CdO) $\approx 411 cm^{-1}$ [19] up to ω_{LO}(ZnO) $\approx 574 cm^{-1}$ [20]. For example, for annealed $Zn_{1-x}Cd_xO$ films with the technologically defined concentration x = 0.12, the Cd concentration determined from the $\Delta\omega$ of A_1^{LO} phonon frequency was about 8%.

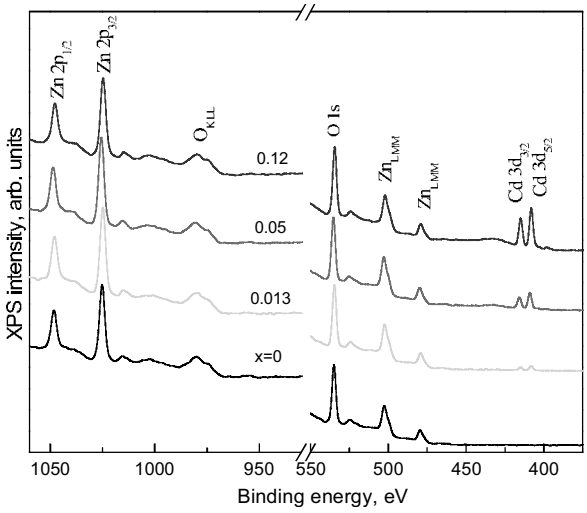

Fig. 2. X-ray photoelectron spectrum of as-grown $Zn_{1-x}Cd_xO$ ternary alloys with the various Cd content.

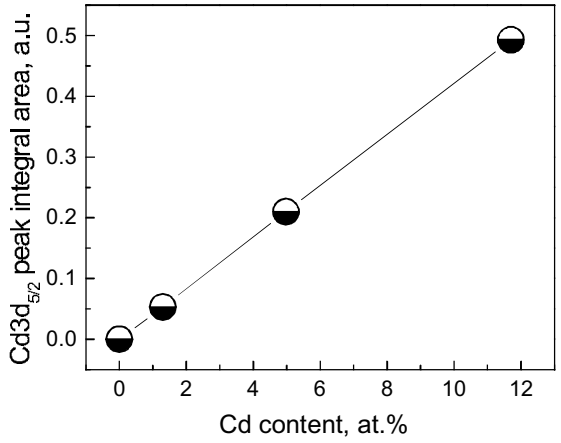

Fig. 3. Dependence of the integral area inherent to the Cd $3d_{5/2}$ peak on the Cd content.

In resonant Raman spectra of as-grown $Zn_{1-x}Cd_xO$ films (Fig. 4a) as compared to undoped ZnO film, the intensity of forbidden single-phonon LO-scattering (1 A_1^{LO}-line) increases substantially. Violation of the conservation law for wave vectors because of violation of translation symmetry in the crystal (existence of structural defects) can be a dominant mechanism of increasing the forbidden 1LO-scattering intensity, while allowable two-photon LO-scattering practically does not depend on structural defects. Therefore, the observed effect of a substantial decrease in the intensity of single-phonon 1 A_1^{LO}-line (by more than 100 times) in the Raman spectrum of annealed $Zn_{1-x}Cd_xO$ films with $x \le 0.05$ can be explained by a significant decrease in the defect concentration, herewith an increase in the intensity of 1 A_1^{LO}-line at $x \ge 0.05$ corresponds to increasing the amount of structural defects.

The non-resonant Raman spectra of as-grown (a) and annealed (b) ZnO and $Zn_{1-x}Cd_xO$ films are shown in Fig. 5. In the Raman spectra of as-grown ZnO film (Fig. 5a), there are well known intense E_2^{low}, E_2^{high} phonon lines at $101.8\,cm^{-1}$ ($\Gamma \approx 3.6\,cm^{-1}$) and at $441.1 cm^{-1}$ ($\Gamma \approx 7.0\,cm^{-1}$) correspondingly [21]. For the E_2^{high} phonon line, the blue shift ($\Delta\omega \approx 4\,cm^{-1}$) occurs as compared with that of monocrystalline ZnO (ω_{bulk}(ZnO) $\approx 437.0\,cm^{-1}$), which is caused by elastic compressive deformations in the film growth plane. In the annealed ZnO film, the E_2^{high} phonon line shifts to the low-energy side to $438.1 cm^{-1}$ ($\Gamma \approx 6.9\,cm^{-1}$) due to partial relaxation of the elastic compressive deformation under thermal annealing. In the non-resonant Raman spectra of both as-grown and annealed ZnO film, the weak A_1^{LO} line was registered at 586.0 and $583.0\,cm^{-1}$, respectively. A weak intensity of the mentioned line is a characteristic feature for the perfect wurtzite ZnO films, which is determined by the processes of destructive interference between the mechanism of Froehlich interaction and deformational potential during scattering by ZnO LO-phonons [22]. Also, in Raman spectra of the as-grown (annealed) ZnO film, the two-phonon line $E_2^{high} - E_2^{low}$ at $334.0\,cm^{-1}$ ($332.8\,cm^{-1}$) was registered.

To quantitatively characterize the influences of strain on optical phonons, the frequency shift of the E_2^{high} mode, $\Delta\omega$, was analyzed as a function of the lateral strain, ε_{xx} [23]:

$$\Delta\omega = 2\left(a - b\frac{C_{13}}{C_{33}}\right)\varepsilon_{xx} = m\cdot\varepsilon_{xx},$$

where $\omega_0 = 437.0\,cm^{-1}$ – E_2^{high} phonon frequency of unstrained ZnO single crystal, $a = -690.8\,cm^{-1}$ and $b = -940\,cm^{-1}$ – phonon deformation potential parameters, C_{13} = 105.1 GPa and C_{33} = 210.9 GPa – elastic constants of ZnO single crystal [24], $m = -443\,cm^{-1}$ is the phenomenological coefficient.

Thereby, the frequency shift $\Delta\omega \approx 4.1\,cm^{-1}$ ($1.1\,cm^{-1}$) of the E_2^{high} phonon line corresponds to deformations $\varepsilon_{xx} \approx -0.0092$ and $\varepsilon_{zz} \approx 0.0105$ ($\varepsilon_{zz} = -\varepsilon_{xx}/0.869$ [23]) in as-grown (annealed) ZnO film, correspondingly.

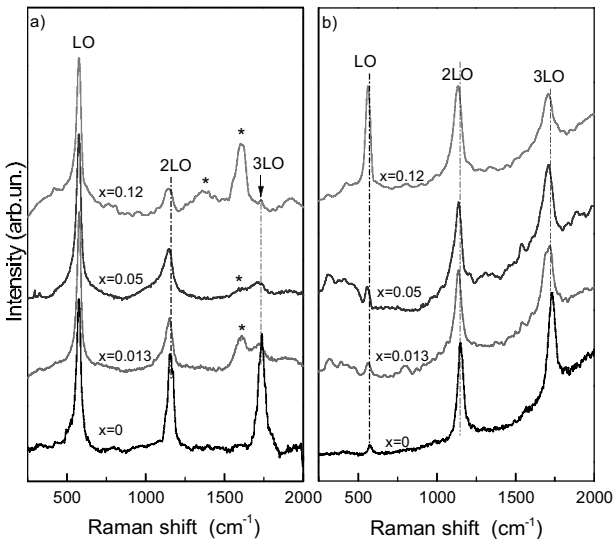

Fig. 4. Resonant Raman spectra of as-grown (a) and annealed (b) $Zn_{1-x}Cd_xO$ films with the various Cd content excited with the wavelength 325 nm (E_{exc} = 3.81 eV). The asterisks mark Raman modes of the carbon clusters. T = 300 K.

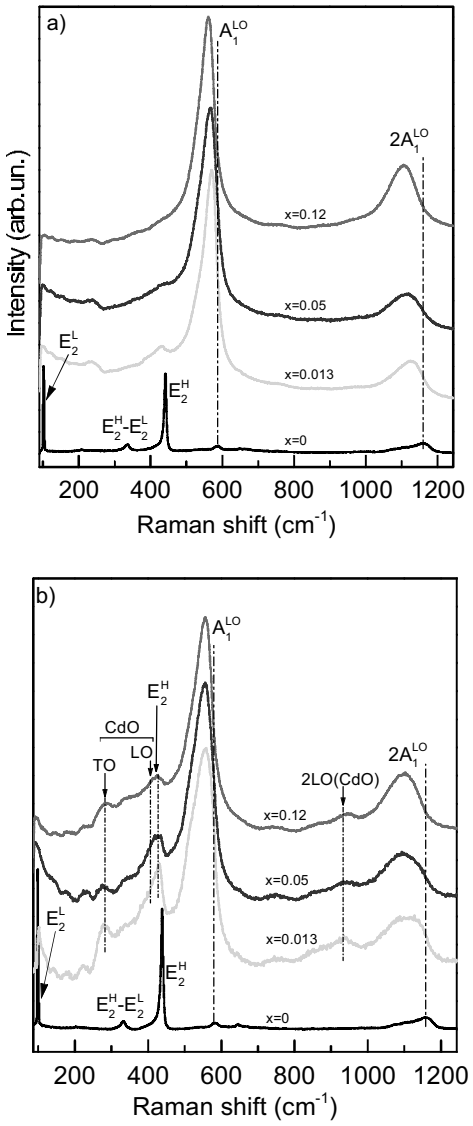

Fig. 5. Non-resonant Raman spectra of as-grown (a) and annealed (b) $Zn_{1-x}Cd_xO$ films with the various Cd content excited with the wavelength 488 nm (E_{exc} = 2.54 eV). T = 300 K.

In the Raman spectra of as-grown $Zn_{1-x}Cd_xO$ films, with the increase in the Cd content we observed a sharp decrease in the intensity and broadening of E_2^{high} phonon line that is caused by structural disorder in the film due to replacement of Zn^{2+} with Cd^{2+} in the host ZnO matrix. With increase in the Cd content to $x = 0.117$, the intensity and FWHM of A_1^{LO}-line increases, and its maximum shifts to the low-frequency side from 586 down to 560.3 cm^{-1} (from 583 to 555.1 cm^{-1}) for as-grown (annealed) $Zn_{1-x}Cd_xO$ film. The low-frequency shift of LO-phonon line relatively to that of bulk ZnO can be attributed to the Cd concentration increase and $Zn_{1-x}Cd_xO$ solid solution formation (taking into account that relaxation of elastic strains leads to the frequency shift of less than 1 cm^{-1}). It is interesting to note that the wide A_1^{LO}-lines in the Raman spectra of $Zn_{1-x}Cd_xO$ can be well decomposed into two Lorentz curves (Fig. 6a). It is related with bimodal distribution of $Zn_{1-x}Cd_xO$ film content. Thus, we can conclude about the existence of two different regions with higher and lower Cd concentration. The high-frequency component of A_1^{LO}-line is assigned to $Zn_{1-x}Cd_xO$ solid solution with small Cd content, while the low-frequency one – to Cd-enriched regions. The data obtained from the analysis of A_1^{LO}-line in the Raman spectra of $Zn_{1-x}Cd_xO$ films are shown in Fig. 6b.

XRD investigations show (Fig. 1) that, under thermal annealing of $Zn_{1-x}Cd_xO$ films, formation of the secondary cubic phase in CdO regions with rocksalt structure occurs. In principle, only the second-order Raman scattering is allowed in rocksalt CdO. Taking into account the results presented in [25], in the Raman spectra of annealed $Zn_{1-x}Cd_xO$ films the scattering caused by existence of CdO rocksalt inclusions was registered (Fig. 5b). Also, the phonon dispersion in CdO was determined: a sharp peak centered at ≈ 280 cm^{-1} is attributed to 2TA(L) second-order mode, a broad feature at about 390 cm^{-1} is caused by the high two-phonon density of states in the 300...450 cm^{-1} frequency region. The weaker Raman mode at ≈ 935 cm^{-1} corresponds to an overtone.

At last, it is worth noting that in the Raman spectra the additional phonon lines at ≈ 1370 and ≈ 1608 cm^{-1} were registered too (in Fig. 4a they are labeled with asterisks). The mentioned lines are attributed to D- and G-lines of amorphous silicon inclusions [26]. Amorphous silicon can contaminate the studied samples during evacuation of the magnetron sputtering system using the oil diffusion pump. After annealing, these peaks disappear (see Fig. 4b), which confirms an assumption about thermal-activated out-diffusion of hydrogen and carbon atoms during the annealing process.

In the spectrum of near-band-edge photoluminescence of as-grown ZnO film (Fig. 7), an intense line of near-band-edge emission at 3.3 eV with FWHM ≈ 80 meV was registered. These line is caused by radiative recombination of localized excitons bounded with neutral donors and/or acceptors [27]. In the PL spectra of as-grown $Zn_{1-x}Cd_xO$ films (Fig. 7, curve 1) at $x = 0.013$, 0.05 and 0.12, weak and substantially broadened ($\Gamma \approx 400$ meV) lines of near-band-edge emission were registered at 3.35, 3.33, and 3.39 eV, respectively. The latter is a strong evidence of

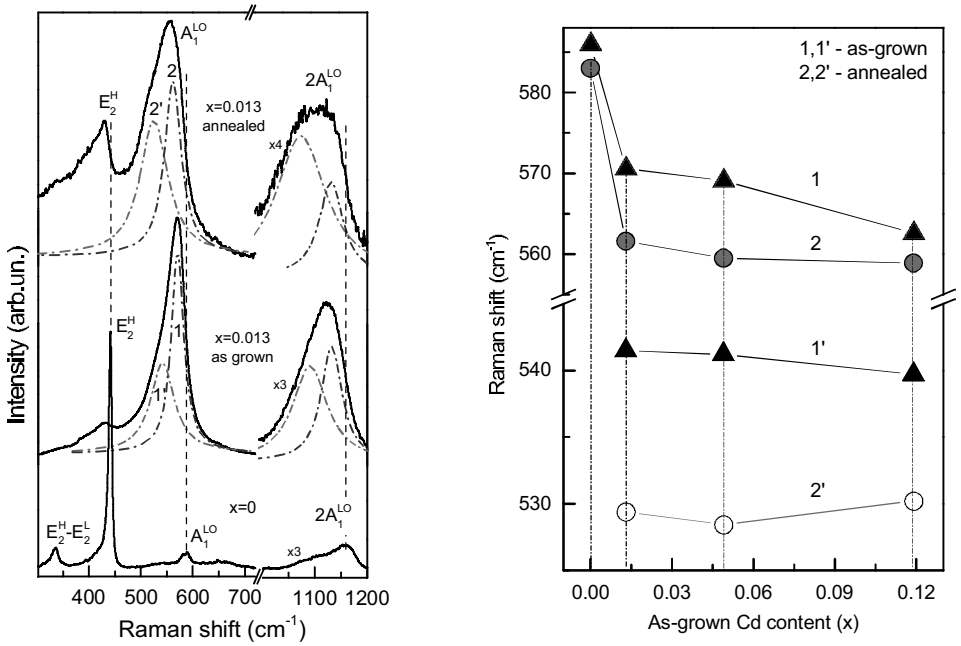

Fig. 6. a) Non-resonant Raman spectra of annealed ZnO film and as-grown and annealed $Zn_{1-x}Cd_xO$ films with x = 0.012. b) Dependence of the frequency of A_1^{LO} -mode on the technologically specified Cd content: *1*, *1'* and *2*, *2'* – low- and high-frequency components of A_1^{LO} -mode.

formation of $Zn_{1-x}Cd_xO$ solid solution and that Cd incorporation leads to significant deterioration of the crystalline structure.

Using the equation for the energy band gap of $Zn_{1-x}Cd_xO$ $E_g^{PL} = 3.28 - 2.23x + 0.45x^2$ [28], the Cd content was determined in the studied $Zn_{1-x}Cd_xO$ structures. It was obtained that for as-grown $Zn_{1-x}Cd_xO$ structures the red shift of the NBE PL line maximum at 0.06 eV corresponds to the change in the Cd content by $\Delta x \approx 3\%$, while technologically specified change of the Cd concentration is about 10%. The latter indicates that during the growth of $Zn_{1-x}Cd_xO$ films the main amount of Cd atoms is not embedded into the crystalline lattice.

The opposite situation is observed for annealed $Zn_{1-x}Cd_xO$ films (T_{ann} = 600 °C). For all the samples with the concentration $x \leq 0.12$, the emission line has two sharp peaks. For example, in the PL spectrum of $Zn_{1-x}Cd_xO$ (x = 0.12), there are two emission lines with shifted towards low energies peak positions – from 3.3 eV (x = 0) down to 2.75 eV (see Fig. 7, curves 2). Herewith, the high-energy line corresponds to the regions depleted of Cd atoms, while the low-energy one – to Cd-enriched regions of $Zn_{1-x}Cd_xO$ solid solution. For the annealed $Zn_{1-x}Cd_xO$ film with the technologically specified Cd concentration x = 0.013, the Cd concentration determined from the peak positions of the PL line at 3.22 and 2.95 eV is equal to x = 0.027 and 0.15, correspondingly. For annealed $Zn_{1-x}Cd_xO$ films with x = 0.05 and 0.12, the

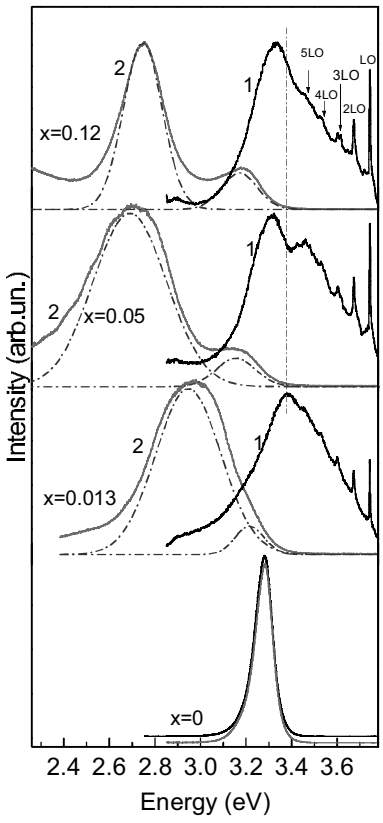

Fig. 7. PL spectra of the as-grown (*1*) and annealed (*2*) $Zn_{1-x}Cd_xO$ films with the various cadmium content. The spectra were deconvoluted using Gaussian fits by the two prominent peaks. E_{exc} = 3.81 eV. T = 300 K.

high-energy PL lines 3.16 and 3.18 eV correspond to the Cd contents equal to $x = 0.055$ and 0.05, while the low-energy lines at 2.69 and 2.75 eV correspond to the Cd contents equal to $x = 0.28$ and 0.25, respectively. Therefore, the Raman scattering and PL investigations of annealed $Zn_{1-x}Cd_xO$ films indicate the existence of two regions – Cd-depleted and Cd-enriched.

4. Conclusions

We investigated the effect of thermal annealing on the structure, vibrational and optical properties of ternary $Zn_{1-x}Cd_xO$ films deposited using the dc reactive sputtering method on (0001) sapphire substrates. XPS measurements clearly confirmed Cd incorporation. XRD patterns enabled to suggest the hexagonal wurtzite structure of the films. XRD pattern obtained from the annealed $Zn_{1-x}Cd_xO$ films with the Cd content higher than 0.013 showed additional peaks from (111), (200) and (220) planes corresponding to CdO, beside hexagonal ZnO peaks. Observation of the E_2^{high} and A_1^{LO} modes in the Raman spectra of the films supports the XRD findings that the films are of good crystallinity and of hexagonal wurtzite structure. With increasing the Cd content of $Zn_{1-x}Cd_xO$ films and their thermal annealing, A_1^{LO} ($Zn_{1-x}Cd_xO$)-like Raman modes showed composition-dependent decrease in frequency and asymmetrical broadening. From the PL measurements, we have obtained that as-grown $Zn_{1-x}Cd_xO$ films with the Cd content $x \le 0.12$ have real amount of Cd atoms incorporated in the crystalline lattice about 30% relatively to technologically specified one. The detailed analysis of near band-edge PL emission and Raman spectrum of the $Zn_{1-x}Cd_xO$ films revealed that in as-grown and annealed films the Cd-depleted and Cd-enriched regions are formed. Consequently, thermal annealing of the $Zn_{1-x}Cd_xO$ films is accompanied with CdO phase segregation.

References

1. Y.-S. Choi, J.-W. Kang, D.-K. Hwang, S.-J. Park, Recent advances in ZnO-based light-emitting diode // *IEEE Trans. Electron. Dev.* **57**, p. 26-41 (2010).
2. O. Madelung, *Semiconductors*: Data Handbook. Springer-Verlag Berlin Heidelberg New York, 3rd edition, 2004.
3. C. Klingshirn, B. Meyer, A. Waag, A. Hoffmann, and J. Geurts, *Zinc Oxide: From Fundamental Properties Towards Novel Applications*, vol. 120. Springer Series in Materials Science, 2010.
4. J. Ishihara, A. Nakamura, S. Shigemori, T. Aoki, and J. Temmyo, $Zn_{1-x}Cd_xO$ systems with visible band gaps // *Appl. Phys. Lett.* **89**, 091914(1-2) (2006).
5. V. Venkatachalapathy, A. Galeckas, M. Trunk, T. Zhang, A. Azarov, and A.Yu. Kuznetsov, Understanding phase separation in ZnCdO by a combination of structural and optical analysis // *Phys. Rev. B*, **83**, 125315(1-11) (2011).
6. F. Bertram, S. Giemsch, D. Forster, and J. Christen, R. Kling and C. Kirchner, A. Waag, Direct imaging of phase separation in ZnCdO layers // *Appl. Phys. Lett.* **88**, 061915(1-3) (2006).
7. L. Li, Z. Yang, Z. Zuo, J.H. Lim, J.L. Liu, Thermal stability of CdZnO thin films grown by molecular-beam epitaxy // *Appl. Surf. Sci.* **256**, p. 4734-4737 (2010).
8. J.H. Yu, J.H. Kim, D.S. Park, T.S. Jeong, C.J. Youn, and K.J. Hong, Effect of rapid thermal annealing on $Zn_{1-x}Cd_xO$ layers grown by radio-frequency magnetron co-sputtering // *Cryst. Res. Technol.* **45**, p. 1050-1056 (2010).
9. P. Klason, T.M. Børseth, Q.X. Zhao, B.G. Svensson, A.Y. Kuznetsov, P.J. Bergman, M. Willander, Temperature dependence and decay times of zinc and oxygen vacancy related photoluminescence bands in zinc oxide // *Solid State Communs*. **145**, p. 321-326 (2008).
10. P.F. Zhang, X.L. Liu, H.Y. Wei, H.B. Fan, Z.M. Liang, P. Jin, S.Y. Yang, C.M. Jiao, Q.S. Zhu, Z.G. Wang, Rapid thermal annealing properties of ZnO films grown using methanol as oxidant // *J. Phys. D: Appl. Phys.* **40**, p. 6010-6013 (2007).
11. A. Ashrafi, K. Ostrikov, Raman-active wurtzite CdO nanophase and phonon signatures in CdO/ZnO heterostructures fabricated by non-equilibrium laser plasma ablation and stress control // *Appl. Phys. Lett.* **98**, 133119(1-3) (2011).
12. Y. Tian, X. Ma, L. Xiang, D. Yang, Electrically pumped simultaneous ultraviolet and visible random laser actions from ZnO-CdO interdiffused film // *Appl. Phys. Lett*. **99**, 261111(1-4) (2011).
13. T. Makino, Y. Segawa, M. Kawasaki, A. Ohtomo, R. Shiroki, K. Tamura, T. Yasuda and H. Koinuma, Band gap engineering based on $Mg_xZn_{1-x}O$ and $Cd_yZn_{1-y}O$ ternary alloy films // *Appl. Phys. Lett.* **78**, p. 1237-1239 (2001).
14. A. Singh, D. Kumar, P.K. Khanna, B.C. Joshia, M. Kumar, Effect of post annealing temperature on structural and optical properties of ZnCdO thin films deposited by sol–gel method // *Appl. Surf. Sci.* **258**, p. 1881-1887 (2011).
15. P. Bartolo-Perez, J.L. Pena and M.H. Farias, El análisis elemental de las superficies de los sólidos mediante las espectroscopiasAuger y de fotoelectrones de rayos X // *Rev. Mex. Fis.* **44**, p. 9-23 (1998).
16. C.A. Arguello, D.L. Rousseau, S.P.S. Porto, First-order Raman effect in wurtzite-type crystals // *Phys. Rev.* **181**, p. 1351-1363 (1969).
17. X. Zhu, H. Wu, Z. Yuan, J. Kong, and W. Shen, Multiphonon resonant Raman scattering in N-

doped ZnO // *J. Raman Spectrosc.* **40**, p. 2155-2161 (2009).
18. V.V. Ursaki, I.M. Tiginyanu, V.V. Zalamai, and E.V. Rusu, G.A. Emelchenko, V.M. Masalov, and E.N. Samarov, Multiphonon resonant Raman scattering in ZnO crystals and nanostructured layers // *Phys. Rev. B*, **70**, 155204(1-8) (2004).
19. R. Oliva, J. Ibanez, L. Artus, R. Cusco, J. Zuniga-Perez, and V. Munoz-Sanjose, High-pressure Raman scattering of CdO thin films grown by metal-organic vapor phase epitaxy // *J. Appl. Phys.* **113**, 053514(1-6) (2013).
20. J.F. Scott, Resonant Raman scattering in ZnO // *Phys. Rev. B*, **2**, p. 1209-1211 (1970).
21. R. Cuscó, E. Alarcón-Lladó, L. Artús, J. Ibáñez, J. Jiménez, B. Wang, and M.J. Callahan, Temperature dependence of Raman scattering in ZnO // *Phys. Rev. B*, **75**, 165202(1-11) (2007).
22. R.H. Callender, S.S. Sussman, M. Selders, and R.K. Chang, Dispersion of Raman cross section in CdS and ZnO over a wide energy range // *Phys. Rev. B*, **7**, p. 3788-3798 (1973).
23. Th. Gruber G.M. Prinz, C. Kirchner, R. Kling, F. Reuss, W. Limmer, A. Waag, Influences of biaxial strains on the vibrational and exciton energies in ZnO // *J. Appl. Phys.* **96**, p. 289-293 (2004).
24. W.-R. Liu, B.H. Lin, C.C. Kuo, W.C. Lee, M. Hong, J. Kwo, C.-H. Hsu and W.F. Hsieh, The influence of dislocations on optical and electrical properties of epitaxial ZnO on Si(111) using a γ-Al_2O_3 buffer layer // *Cryst. Eng. Communs.* **14**, p. 8103-8109 (2012).
25. R. Cuscó, J. Ibáñez, N. Domenech-Amador, L. Artús, J. Zúñiga-Pérez and V. Muñoz-Sanjosé, Raman scattering of cadmium oxide epilayers grown by metal-organic vapor phase epitaxy // *J. Appl. Phys.* **107**, 063519 (1-4) (2010) .
26. G. Katumba, B.W. Mwakikunga, T.R. Mothibinyane, FTIR and Raman spectroscopy of carbon nanoparticles in SiO_2, ZnO and NiO matrices // *Nanoscale Res. Lett.* **3**, p. 421-426 (2008).
27. Y.W. Chen, Y.C. Liu, S.X. Lu, C.S. Xu, C.L. Shao, C. Wang, J.Y. Zhang, Y.M. Lu, D.Z. Shen, X.W. Fan, Optical properties of ZnO and ZnO:In nanorods assembled by sol-gel method // *J. Chem. Phys*. **123**, 134701(1-5) (2005).
28. A. Buyanova, X.J. Wang, W.M. Chen, M. Izadifard, D.P. Norton, S.J. Pearton, A. Osinsky, J.W. Dong and A. Dabiran, Optical characterization of $Zn_{1-x}Cd_xO$ alloys grown by molecular-beam epitaxy // *ECS Trans*. **3**, p. 391-398 (2006).